J. Phase Equilib. Diffus. (2022) 43:576–584
https://doi.org/10.1007/s11669-022-01000-4

Phase Equilibria of the Mg-Sn-Pr Ternary System at 500 °C

Zhongtao Wei[1] · Shengyu Liu[1] · Jingxian Wen[1] · Cuiyun He[1]

Submitted: 7 June 2022 / in revised form: 8 September 2022 / Accepted: 12 September 2022 / Published online: 23 November 2022

Abstract The phase equilibria of the Mg-Sn-Pr ternary system at 500 °C were investigated by x-ray power diffraction (XRD), scanning electron microscope equipped with energy dispersive spectrometer (SEM–EDS). Seven ternary phases were observed. The crystal structure for the phases: τ_1 ($MgSnPr$, *I4/mmm*, *tI*12) and τ_2 ($MgSn_2Pr$, *I42m*, *tI*32) were confirmed to exist at this temperature. Five new ternary compounds τ_3 to τ_7 are stable at 500 °C. Their compositions have been determined, but their crystal structures are still under investigation. The solubility of Mg in $PrSn_3$, αPr_3Sn_5 and $PrSn_3$ is about 2, 2 and 11 at.% Mg, respectively. The MgPr shows a solubility of 5.7 at.% Sn.

Keywords experimental phase equilibria · Mg-Sn-Pr ternary system · Mg-Sn-Rare earth alloy

1 Introduction

Magnesium alloys are considered promising alternatives to conventional metal alloys (Al alloys, Ti alloys and steel, etc.) for automotive and aerospace applications due to their low density ($\sim$ 1.7 g/cm^3), high specific strength, good castability and availability.[1–3] However, the relatively low creep resistance at elevated temperature of Mg alloys is regarded as the key challenge limiting their wider application in automotive and aerospace industries since some critical components are used at temperatures above 175 °C.[4] Adding alloying elements is an effective way to strengthen Mg alloys. Sn is a promising age-hardening element for Mg since its solid solubility in Mg matrix varies greatly with temperature and Mg_2Sn is a thermally stable phase.[5] Nevertheless, the Mg_2Sn particles that form in Mg matrix are larger, thus reducing the age-hardening response of the alloys.[6] Rare earth (RE) metals are another important alloying element of Mg alloys. Studies have found that Mg alloys with RE elements have good corrosion resistance, high strength, excellent creep resistance and better deformability.[7–9] Lim et al. reported that a small amount of Sn can enhance the ductility in Mg-rich Mg-MM (misch-metal) alloys.[10] In order to find a new creep-resistant Mg alloys, the knowledge of phase equilibria in Mg-Sn-RE systems is of fundamental importance. Up to now, the phase equilibria of the Mg-Sn-Pr ternary system have not been reported yet. The purpose of present work is to experimentally investigate the phase equilibria of the Mg-Sn-Pr system at 500 °C in equilibrated alloys using x-ray diffraction (XRD) and scanning electron microscope equipped with energy dispersive spectrometer (SEM/EDS). The obtained phase diagram is expected to provide useful information for novel Mg alloy design.

2 Literature Review

The Mg-Sn and Mg-Pr binary phase diagrams were adopted from the book of Massalski,[11] which was based on the evaluated diagrams by Nayeb-Hashemi and Clark.[5,12] There is only one binary compound Mg_2Sn in the Mg-Sn system, and it is congruently formed from liquid at 770 °C. The Mg-Pr system has five binary compounds: $Mg_{12}Pr$, $Mg_{41}Pr_5$, Mg_3Pr, Mg_2Pr and $MgPr$. Mg_2Pr is stable at high

✉ Cuiyun He
hcy_2003@hotmail.com

[1] Guangxi Key Laboratory of Processing for Nonferrous Metal and Featured Materials, School of Resources Environment and Materials, Guangxi University, Nanning, Guangxi, People's Republic of China

temperature and decomposes at 670 °C. The Pr-Sn binary system is complex due to the high oxidizability of Pr-Sn alloys. The Pr-Sn phase diagram reported by Eremenko et al. [13] and reproduced by Massalski [11] contains eight compounds: Pr_3Sn, αPr_5Sn_3, βPr_5Sn_3, Pr_5Sn_4, PrSn, αPr_3Sn_5, βPr_3Sn_5 and $PrSn_3$. Subsequently, the $PrSn_2$, Pr_3Sn_7, Pr_2Sn_5 and Pr_2Sn_3 phases were reported by several researchers.[14–16] The phase diagram of the Pr-Sn binary system was assessed by Kim et al. using the Calphad method.[17] It contains 13 binary compounds and was adopted in the present work. In the Mg-Sn-Pr ternary system, two ternary phases, i.e., τ_1-MgSnPr and τ_2-$MgSn_2Pr$, were reported.[18,19] The three binary boundary phase diagrams and the two ternary compounds are shown in Fig. 1 and the crystallographic data for all unary and binary solid phases in the Mg-Sn-Pr system are listed in Table 1.

3 Experimental Procedure

High-purity metal nuggets: Mg 99.5, Sn 99.5 and Pr 99.5 wt. % were used as starting materials. More than 30 ternary alloys were synthesized in the ternary system. Several steps were taken in the preparation procedure. First, small pieces of the starting materials were weighed and put into tantalum tubes. Then these Ta tubes were sealed in an enclosed chamber filled with argon. Subsequently, the sealed Ta tubes were sealed into evacuated quartz tubes. Finally, these double-sealed samples were

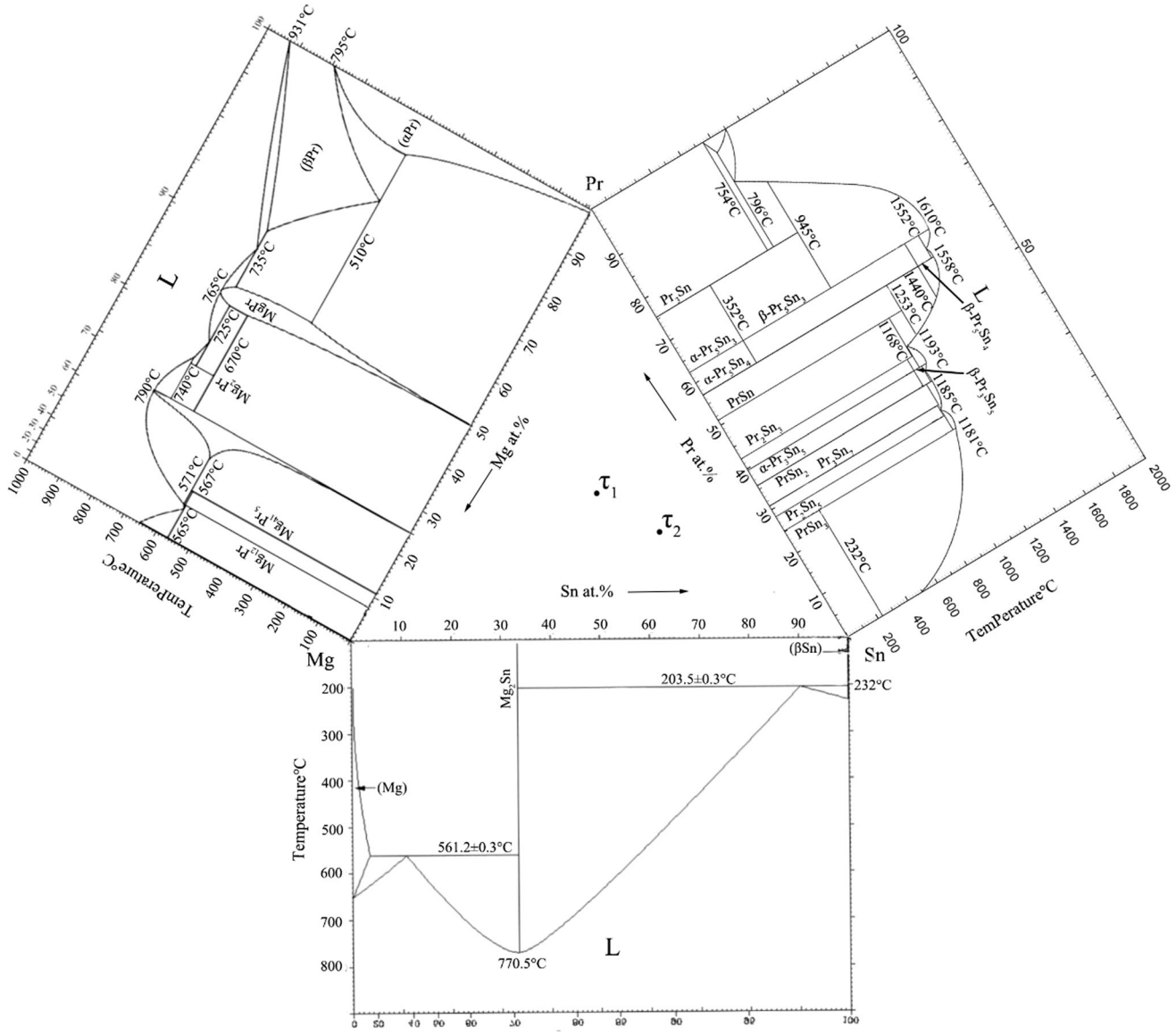

Fig. 1 Binary phase diagrams constituting the Mg-Sn-Pr ternary system

Table 1 Crystallographic data for the unary and binary phases in the Mg-Sn-Pr system

Phase	Pearson symbol	Space group	Prototype	Strukturbericht type	Ref
(Mg)	*hP*2	*P6*$_3$*/mmc*	Mg	A3	5
(βSn)	*tI*4	*I4*$_1$*/amd*	βSn	A5	5
(αSn)	*cF*8	*Fd-3 m*	C (diamond)	A4	5
Mg_2Sn	*cF*12	*Fm3m*	CaF_2	C1	5
(αPr)	*hP*4	*P6*$_3$*/mmc*	αLa	A3'	12
(βPr)	*cI*2	*Im-3 m*	W	A2	12
$Mg_{12}Pr$	*tI*26	*I4/mmm*	$Mn_{12}Th$	$D2_b$	12
$Mg_{41}Pr_5$	*tI*92	*I4/m*	$Mg_{41}Ce_5$	…	12
Mg_3Pr	*cF*16	*Fm-3 m*	BiF_3	$D0_3$	12
Mg_2Pr	*cF*24	*Fd-3 m*	Cu_2Mg	C15	12
MgPr	*cP*2	*Pm-3 m*	CsCl	B2	12
Pr_3Sn	*cP*4	*Pm-3 m*	$AuCu_3$	$L1_2$	11
Pr_2Sn_5	*oC*28	*Cmmm*	Ce_2Sn_5	…	16
Pr_3Sn_7	*oC*20	*Cmmm*	Ce_3Sn_7	…	16
$PrSn_2$	*oC*12	*Cmmm*	$ZrGa_2$	…	16
Pr_2Sn_3	…	…	…	…	16
$Pr_{11}Sn_{10}$	…	…	…	…	16
βPr_5Sn_3	*hP*16	*P6*$_3$*/mcm*	Mn_5Si_3	$D8_8$	11
αPr_5Sn_3	*tI*32	*I4/mcm*	W_5Si_3	$D8_m$	11
Pr_5Sn_4	*oP*36	*Pnma*	Sm_5Ge_4	…	11
PrSn	*oP*8	*Pnma*	FeB	B27	11
βPr_3Sn_5	…	…	…	…	11
αPr_3Sn_5	…	…	…	…	11
$PrSn_3$	*cP*4	*Pm-3 m*	$AuCu_3$	$L1_2$	11

melted in a resistance furnace through the following process: the resistance furnace was heated to 600 °C and held for one hour, then the temperature was increased to 750 °C and held for two hours, and finally the temperature was raised to 820 °C and held for two days. At 820 °C, the sealed tubes with the samples were turned upside-down every few hours in order to homogenize the samples. After being melted, these samples were annealed at 500 °C for 45 days, followed by ice water quenching.

Phase identification was done by x-ray diffraction (XRD) with Cu-Kα radiation at 40 kV and a current of 40 mA (D8 Discover X, BRUKER, Germany). It should be mentioned that a small amount of paraffin was added to prevent the oxidation of the samples when the samples were ground into powder and characterized/analyzed by XRD. Phase compositions were determined by energy dispersive spectroscopy (EDS) analyzer (Oxford X-MAX80 Britain) attached to a field-emission scanning electron microscope (HitachiSU-8000 Japan). The compositions of each phase were obtained from the average value of 5-10 measured EDS data. It should be noted that the metallographic samples were ground with anhydrous alcohol initially and with anhydrous polishing agent at end to avoid any possible reaction of Mg and Pr with water. The prepared metallographic samples were first stored in anhydrous alcohol, and then taken to a vacuum glove box, where they were removed from the alcohol, after being dried out and sealed in a vacuum plastic bag waiting microscopic inspection.

4 Results and Discussion

4.1 Microstructure and Phase Equilibria

In the present work, the compositions of the phases in equilibrated alloys at 500 °C were measured by EDS, and their crystal structures were analyzed by XRD. The chemical compositions are given in atomic ratio (at.%). The microstructure of selected samples are shown on Fig. 2(a-f) and two XRD patterns containing ternary compounds τ_2 and τ_3 are presented in Fig. 3(a-b).

The SEM picture of 1# alloy ($Mg_{74.9}Sn_{10.6}Pr_{14.5}$) provides key experimental evidence that τ_5 ($Mg_{44.6}Sn_{24.2}Pr_{31.2}$) is a different phase compared to τ_1($Mg_{35.7}Sn_{33.2}Pr_{31.1}$). The colors of the two phases are so close that they cannot be easily distinguished from each other. However, a phase boundary can be observed at the

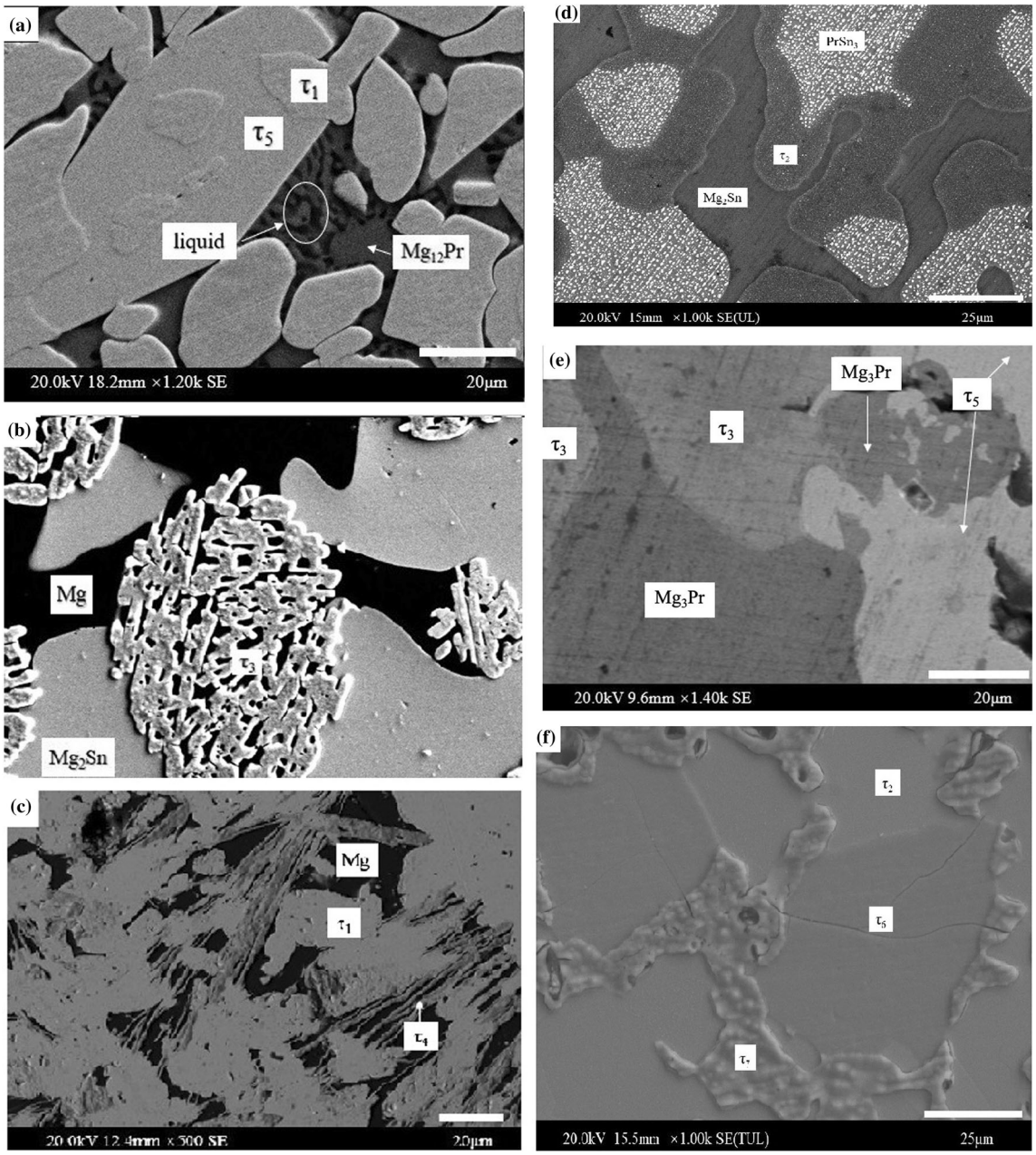

Fig. 2 Typical SEM images obtained from equilibrium alloys annealed at 500 °C for 45 days: (a) 1# alloy ($Mg_{74.9}Sn_{10.6}Pr_{14.5}$) showing coexistence of τ_1 (grey, $Mg_{35.7}Sn_{33.2}Pr_{31.1}$) + τ_5 (grey, $Mg_{44.6}Sn_{24.2}Pr_{31.2}$) + Liq ($Mg_{12}Pr$ + (Mg) eutectic structure); (b) 2# alloy ($Mg_{67.5}Sn_{27}Pr_{5.5}$) showing coexistence of (Mg) (dark) + τ_4 (mesh, $Mg_{55.5}Sn_{27.5}Pr_{17}$) + Mg_2Sn (light grey); (c) 3# alloy ($Mg_{75.4}Sn_{12.6}Pr_{12}$) showing coexistence of τ_1 (blocky grey, $Mg_{33.3}Sn_{33.3}Pr_{33.4}$) + (Mg) (black) + τ_4 (needle-like grey, $Mg_{59}Sn_{24}Pr_{17}$); (d) 4# alloy ($Mg_{20.1}Sn_{58.6}Pr_{21.3}$) showing coexistence of Mg_2Sn (black) + τ_2 (grey, $Mg_{26.2}Sn_{52.7}Pr_{21.1}$) + $PrSn_3$ (light grey, $Mg_{11.1}Sn_{65.2}Pr_{23.7}$); (e) 5# alloy ($Mg_{65.2}Sn_{8.1}Pr_{26.7}$) showing coexistence of τ_5 (light grey, $Mg_{41.3}Sn_{23.1}Pr_{35.6}$) + τ_3 (grey, $Mg_{75.2}Sn_{2.3}Pr_{22.5}$) + Mg_3Pr (deep grey, $Mg_{74.2}Sn_{0.1}Pr_{25.7}$); (f) 22# alloy ($Mg_{30}Sn_{41.7}Pr_{28.3}$) showing coexistence three phases, τ_2 (light grey, $Mg_{21}Sn_{51.1}Pr_{26.9}$) + τ_6 (grey, $Mg_{38}Sn_{37}Pr_{25}$) + τ_7 grey phase with a rough surface, $Mg_{20}Sn_{45}Pr_{35}$)

junction of the two phases. It is necessary to state that the 1# alloy is not a fully equilibrated alloy since the (Mg) + $Mg_{12}Pr$ eutectic structure still exists in the alloy. In Fig. 2(b, a) three-phase microstructure of (Mg) + τ_4 + Mg_2Sn is observed for 2# alloy ($Mg_{67.5}Sn_{27}Pr_{5.5}$). The grey phase is Mg_2Sn, and the black phase is (Mg). The composition of the grey network is $Mg_{55.5}Sn_{27.5}Pr_{17}$, which we as assumed to be a new ternary compound and named it τ_4. Figure 2c shows a three phases field of τ_1 + τ_4 + (Mg) in 3# alloy ($Mg_{75.4}Sn_{12.6}Pr_{12}$). The large blocky grey phase is τ_1 and the black phase is (Mg). The composition of the acicular grey phase is $Mg_{59}Sn_{24.0}Pr_{17}$, which is like the τ_4

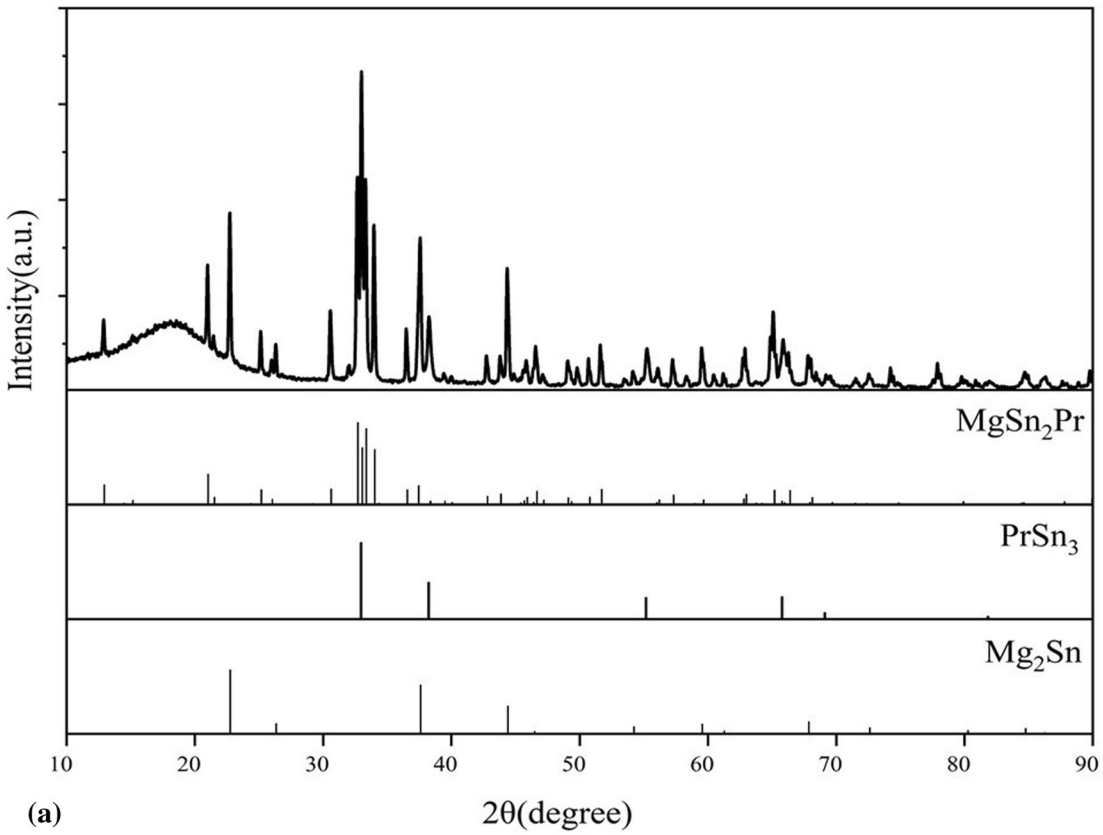
Intensity(a.u.)
MgSn2Pr
PrSn3
Mg2Sn
10
20
30
40
50
60
70
80
90
2θ(degree)

(a)

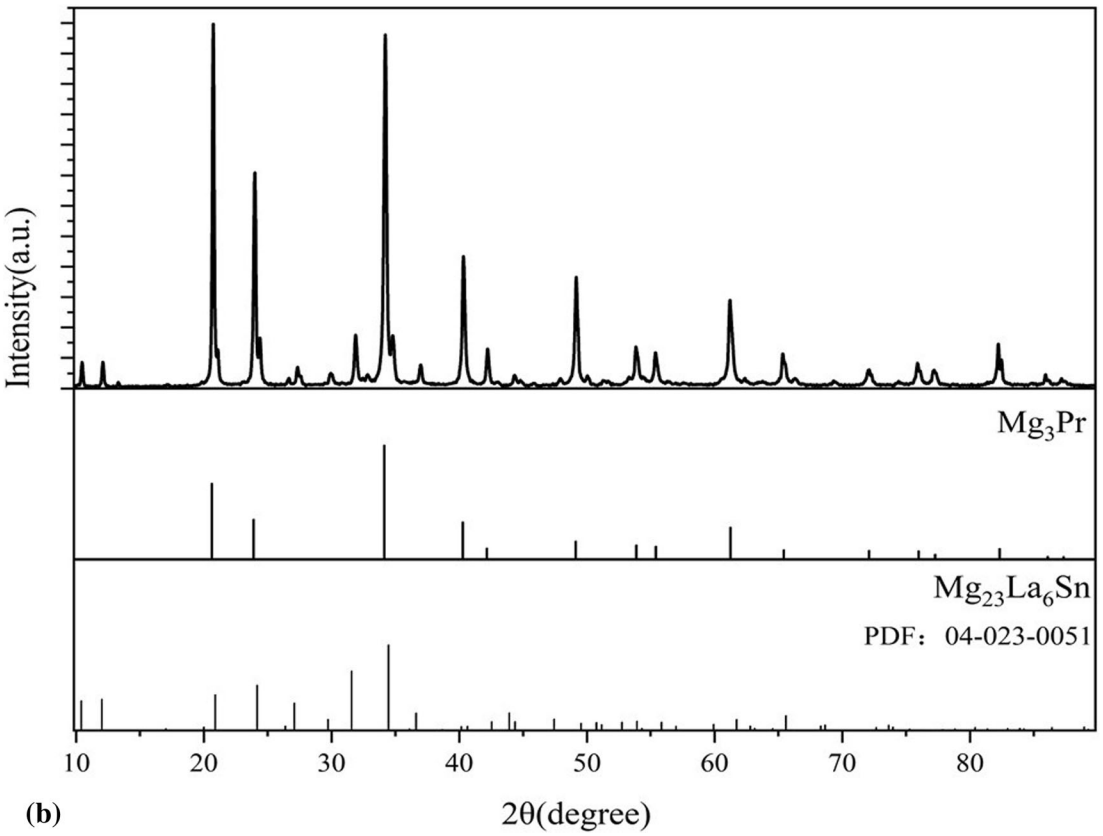
Intensity(a.u.)
Mg3Pr
Mg23La6Sn
PDF：04-023-0051
10
20
30
40
50
60
70
80
2θ(degree)

(b)

◀**Fig. 3** X-ray diffraction patterns of (a) 4# alloy ($Mg_{20.1}Sn_{58.6}Pr_{21.3}$) showing coexistence of three phase, τ_2, Pr_3Sn and Mg_2Sns; (b) 14# alloy ($Mg_{75.2}Sn_1Pr_{23.8}$) showing that it contains Mg_3Pr and a phase with the same structure as $Mg_{23}SnLa_6$. The vertical marks indicate the positions of possible Bragg reflections of each phase in the studied alloys

of 2# alloy (Fig. 2b). Currently, we believe that both phases are the same ternary compound τ_4: $Mg_{59-x}Sn_{24+x}Pr_{17}$ ($x = 0 \sim 3.5$), and Mg and Sn have a certain mutual solubility due to the relatively close compositions of these two phases and the lack of key high-quality XRD patterns.

The 4# ($Mg_{20.1}Sn_{58.6}Pr_{21.3}$) alloy shows three distinct phases in Fig. 2(d). Whilst the dark phase and large grey phase could be identified as Mg_2Sn and τ_2 ($Mg_{26.2}Sn_{52.7}Pr_{21.1}$) by EDS analysis, the composition of large light grey is $Mg_{11.1}Sn_{65.2}Pr_{23.7}$ is difficult to determine and whether this phase is a new ternary phase or a binary phase with a solid solubility. The XRD pattern of the alloys (Fig. 3a) reveals the answer, in it the $PrSn_3$ phase can be identified as well as the characteristic peaks of Mg_2Sn and τ_2 phases. In other words, $PrSn_3$ dissolves up to 11 at.% Mg. As mentioned in the experimental procedure, paraffin oil was added to the samples during grinding and XRD analysis to slow down the oxidation rate of samples. Therefore, an amorphous hump could be observed at the low angle region in XRD pattern of sample. In addition, the surface of $PrSn_3$ was covered with some small particles which turns out to be Rare Earth Oxide (REO). They were produced from an air exposure within two minutes, which occurred while the alloy was transferred to the scanning electron microscopy equipment.

The microstructure of 5# alloy ($Mg_{65.2}Sn_{8.1}Pr_{26.7}$) in Fig. 2(e) shows the coexistence of three phases, the light grey phase is τ_5 ($Mg_{41.3}Sn_{23.1}Pr_{35.6}$) and the large dark grey phase is Mg_3Pr. The color of third phase is lighter than Mg_3Pr and darker than τ_5. The composition of third phase is $Mg_{75.2}Sn_{2.3}Pr_{22.5}$, which is close to the composition of Mg_3Pr ($Mg_{74.2}Sn_{0.1}Pr_{25.7}$). But obviously, it is a different phase from Mg_3Pr since Mg_3Pr hardly contains solid solubility of Sn, and we named it τ_3. Figure 3(b) shows the XRD pattern of the 14# alloy located between $MgPr_3$ and τ_3 matched well the characteristic peaks of $Mg_{23}SnLa_6$ phase (ICDD, PDF 04–023-0051) and the peaks of Mg_3Pr phase. It seems that τ_3 is an isostructural with $Mg_{23}SnLa_6$. ($Zr_6Zn_{23}Si$ prototype, *cF*120 Pearson symbol)[20]. The microstructure of 22# alloy contains three distinct phases as shown in Fig. 2(f). The light grey phase is τ_2 ($Mg_{21}Sn_{51.1}Pr_{26.9}$). The grey phase with a rough surface has a new composition as $Mg_{20}Sn_{45}Pr_{35}$ and was named τ_7. The grey phase in the middle layer with another new composition ($Mg_{38}Sn_{37}Pr_{25}$) was named τ_6.

4.2 Isothermal Section at 500 °C

Experimental data of EDS and XRD obtained from selected equilibrium alloys, which have been annealed at 500 °C for 45 days, are summarized in Table 2. The isothermal section at 500 °C constructed based on these data is shown in Fig. 4 with symbols indicating the alloy compositions. It should be noted that the 5 alloys (18#-22#) located in the regions (βPr_5Sn_3-τ_1-τ_6-τ_2-$PrSn_3$) near the Pr-Sn boundary system were only examined by SEM/EDS and not by XRD, due to the high oxidizability of Pr-Sn alloys. The phase regions without experimental data, which were estimated from the surrounding phase relationship, are indicated with dashed lines.

The binary phases show different ranges of solubility with respect to the third element in the system. The solid solubilities of Mg in Pr_3Sn, βPr_5Sn_3 and $PrSn_3$ are 2, 2 and 11 at.%, respectively. The MgPr compound shows a solubility of 5.7 at.% Sn. Other Pr-Sn and Mg-Pr binary compounds show no appreciable Mg or Sn solubility. The solubilities of αPr_5Sn_4, PrSn, $PrSn_2$ and αPr_3Sn_5 are shown as the dashed lines since they are simply deduced from the EDS data from alloys near them.

Within the regions that have been studied, seven ternary compounds were observed at 500 °C. Their homogeneity ranges and crystal structures are listed in Table 3. Two known ternary compounds τ_1 (MgSnPr, *I4/mmm*, *tI*12) and τ_2 ($MgSn_2Pr$, *I42m*, *tI*32) were detected at 500 °C. Five new compounds were named as τ_n, with n ranging from 3 to 7 with decreasing of Mg content. Figure 3b shows that τ_3 may have the same structure as $Mg_{23}SnLa_6$. ($Zr_6Zn_{23}Si$ prototype, *cF*120 Pearson's code)[20]. The evidence for the existence of the other four new ternary compounds is mainly based on SEM/EDS data. The crystal structures of τ_4 to τ_7 have not been determined yet, since high-quality XRD patterns of these new ternary compounds are still

Table 2 Phase identification (by EDS and XRD) of equilibrated Mg-Sn-Pr alloys at 500 °C

Alloy	Alloy Composition (at.%)			Phase	Phase composition (at.%)			Figure
	Mg	Sn	Pr		Mg	Sn	Pr	
1(a)	74.9	10.6	14.5	$(\tau_5)^b$	44.6	24.2	31.2	Figure 2(a)
	…	…	…	τ_1	35.7	33.2	31.1	…
	…	…	…	(Mg) + $Mg_{12}Pr$	93.4	1.4	5.2	…
2	67.5	27.0	5.5	Mg_2Sn	63.6	36.4	0.0	Figure 2(b)
	…	…	…	(τ_4)	55.5	27.5	17	…
	…	…	…	Mg	97.3	2.6	0.1	…
3	75.4	12.6	12.0	Mg	99.7	0.2	0.1	Figure 2(c)
	…	…	…	τ_1	33.3	33.3	33.4	…
	…	…	…	(τ_4)	59.0	24.0	17.0	…
4	20.1	58.6	21.3	$PrSn_3$	11.1	65.2	23.7	Figure 2(d)
	…	…		τ_2	26.2	52.7	21.1	Figure 3(a)
	…	…	…	Mg_2Sn	62.6	35.5	1.9	…
5	65.2	8.1	26.7	(τ_5)	41.3	23. 1	35.6	Figure 2(e)
	…	…	…	(τ_3)	75.2	2.3	22.5	…
	…	…	…	Mg_3Pr	74.2	0.1	25.7	…
6	72.6	6.3	21.1	(τ_5)	42.6	23.4	34.0	…
	…	…	…	(τ_3)	75.0	4.0	21.0	…
	…	…	…	$Mg_{41}Pr_5$	88.3	0.1	11.6	…
7	92.8	3.9	3.3	τ_1	35.4	32.2	32.4	…
	…	…	…	Mg	99.9	0.1	0	…
8	54.9	11.9	33.6	(τ_5)	41.2	22.5	36.3	…
	…	…	…	Mg_3Pr	73.0	0.3	26.7	…
	…	…	…	βPr_5Sn_3	2.8	36.5	60.4	…
9	19.3	21.7	59.0	βPr_5Sn_3	0.8	36.1	63.1	…
	…	…	…	Pr_3Sn	4.8	22.7	72.5	…
	…	…	…	MgPr	43.4	5.6	51.0	…
10	38.3	17.7	44	βPr_5Sn_3	1.9	36.6	61.5	…
	…	…	…	Mg_3Pr	73.9	0.3	25.8	…
	…	…	…	MgPr	47.4	3.1	49.5	…
11	18.5	64.5	16.9	$PrSn_3$	2.4	72.2	25.5	…
	…	…	…	Liq (Sn)	24.2	73.5	2.3	…
	…	…	…	Mg_2Sn	65.1	34.3	0.6	…
12	38.8	47.9	11.3	$PrSn_3$	11.7	63.3	25	…
	…	…	…	τ_2	25.3	49.4	25.3	…
	…	…	…	Mg_2Sn	63.7	36.2	0.1	…
13	32.9	27.1	40.0	βPr_5Sn_3	2.2	36.4	61.4	…
	…	…	…	(τ_5)	41.1	23.0	35.9	…
14	75.2	1	23.8	Mg_3Pr	75.2	0.2	24.6	Figure **3(b)**
	…	…	…	τ_3	75.3	2.1	22.6	…
15	15.7	11.7	72.6	(Pr)	1.0	0.4	98.6	…
	…	…	…	Pr_3Sn	1.8	23.4	74.8	…
	…	…	…	MgPr	46.6	1.0	52.3	…
16	82.3	7.0	10.7	(τ_5)	33.1	33.3	33.6	…
	…	…	…	$Mg_{12}Pr$	91.5	0.0	8.5	…
	…	…	…	(Mg)	99.6	0.1	0.3	…

Table 2 continued

Alloy	Alloy Composition (at.%)			Phase	Phase composition (at.%)			Figure
	Mg	Sn	Pr		Mg	Sn	Pr	
17	75.8	11.9	12.3	τ_1	33.1	33.4	33.5	…
	…	…	…	$Mg_{12}Pr$	91.5	0.11	8.32	…
	…	…	…	(Mg)	99.6	0.1	0.3	…
18*	15.3	34.8	49.9	(τ_5)	42	24	34	
	…	…	…	Pr_5Sn_3	0.8	37.6	61.6	…
	…	…	…	Pr_5Sn_4 ?	5.5	38.9	55.6	…
19*	13.2	59.2	27.6	τ_2	24.1	50.1	25.8	…
	…	…	…	$PrSn_2$?	4.4	64.6	31.0	…
	…	…	…	$PrSn_3$	11.4	63.2	25.4	…
20*	18.3	38.6	43.1	τ_1	33.2	33.4	33.4	…
	…	…	…	PrSn ?	8	42.5	49.5	…
	…	…	…	Pr_5Sn_4 ?	6	38.8	55.2	…
21*	9.3	59.5	31.2	τ_2	24.2	50	25.8	…
	…	…	…	$PrSn_2$?	5.4	64.5	30.2	…
	…	…	…	Pr_3n_5 ?	1.5	60.9	37.6	…
22*	30	41.7	28.3	(τ_2)	21	51.1	26.9	Figure 2(f)
	…	…	…	(τ_6)	38	37	25	…
	…	…	…	(τ_7)	20	45	35	…

(a) The 1# alloy is non-equilibrium since it contains eutectic structure of (Mg) + $Mg_{12}Pr$.

(b) The τ_4, τ_5, τ_6 and τ_7 phases are enclosed in parenthesis since they were not identified by XRD.

*: The samples marked with * were only examined by SEM/EDS and not by XRD.

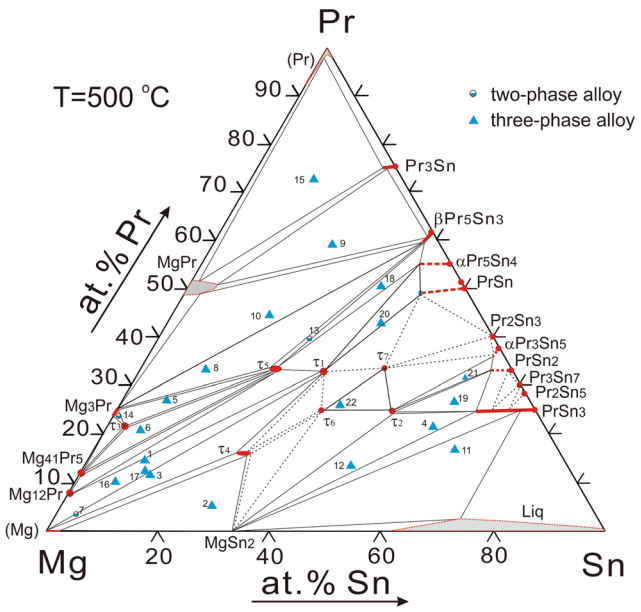

Fig. 4 Experimental isothermal section of the Mg-Sn-Pr system at 500 °C

lacking. However, by comparing with the isothermal section of La-Mg-Sn system at 500 °C from the literature [20], we have found that except for τ_4 ($Mg_{59-x}Sn_{24+x}Pr_{17}$, $x = 0 \sim 4$), the composition ratios of τ_5($Mg_{40-44}Sn_{26.5-22.5}Pr_{33.5}$), τ_6($Mg_{38}Sn_{37}Pr_{25}$) and τ_7($Mg_{20}Sn_{45}Pr_{35}$) are like the ternary compounds ($Mg_{4-x}Sn_{2+x}La_3$ $0.12 < x \leq 0.4$, $Mg_{35}Sn_{40}La_{25}$ and $Mg_{20}Sn_{45}La_{35}$) in the La-Mg-Sn system.

5 Conclusions

The 500 °C isothermal section of the Mg-Sn-Pr ternary system was determined by SEM with EDX and XRD. The main findings are as follow:

(i) Within the investigated regions, τ_1 (MgSnPr) and τ_2 ($MgSn_2Pr$), and five new ternary compounds (τ_3, τ_4, τ_5, τ_6 and τ_7) were observed in the section. Except for τ_4 phase, the τ_3, τ_5, τ_6 and τ_7 have same or similar composition ratios as four ternary compounds in La-Mg-Sn system.

Table 3 Ternary compounds in the Mg-Sn-Pr system at 500 °C

Phase	Pearson symbol	Space group	Prototype	Ref	Comments
τ_1-MgSnPr	*tI*12	*I4/mmm*	MgSnCe	18	…
τ_2-$MgSn_2Pr$	*tI*32	*I-42 m*	$MgSn_2La$	19	…
$\tau_3 \sim Mg_{75}Sn_{2.5-4}Pr_{22.5-21}$	Unknown			TW	Its composition ratio and XRD pattern are similar to $Mg_{23}SnLa_6$ [20]
$\tau_4 \sim Mg_{55.5-59}Sn_{27.5-24}Pr_{17}$	Unknown			TW	…
$\tau_5 \sim Mg_{40-44}Sn_{26.5-22.5}Pr_{33.5}$	Unknown			TW	Its composition ratio is similar to $Mg_{4-x}Sn_{2+x}La_3$ $0.12 < x \leq 0.4$ [20]
$\tau_6 \sim Mg_{38}Sn_{37}Pr_{25}$	Unknown			TW	$Mg_{35}Sn_{40}La_{25}$ [20]
$\tau_7 \sim Mg_{20}Sn_{45}Pr_{35}$	Unknown			TW	$Mg_{20}Sn_{45}La_{35}$ [20]

TW This work.

(ii) At 500 °C, Pr_3Sn, βPr_5Sn_3 and $PrSn_3$ show a solubility of 2, 2 and 11 at.% Mg, respectively. The solubility of Sn in MgPr is 5.7 at.%.

Acknowledgments Financial support from the National Natural Science Foundation of China under the project number (No. 51061003, No. 51461005) and MOE Key Laboratory of New Processing Technology for Non-ferrous Metals and Materials of Guangxi University (2021GXMPSF) are gratefully acknowledged.

References

1. F. Pan, M. Yang, and X. Chen, A Review on Casting Magnesium Alloys: Modification of Commercial Alloys and Development of New Alloys, *J. Mater. Sci. Technol.*, 2016, **32**, p 1211–1221.
2. B.L. Mordike and T. Ebert, Magnesium: Properties—applications—potential, *Mater. Sci. Eng. A*, 2001, **302**, p 37–45.
3. S.V.S. Prasad, S.B. Prasad, K. Verma, R.K. Mishra, V. Kumar, and S. Singh, The role and significance of Magnesium in Modern Day Research-A Review, *J. Magnes. Alloys*, 2022, **10**, p 1–61.
4. N. Mo, Q. Tan, M. Bermingham, Y. Huang, H. Dieringa, N. Hort et al., Current Development of Creep-Resistant Magnesium Cast Alloys: A Review, *Mater. Des.*, 2018, **155**, p 422–442.
5. A.A. Nayeb-Hashemi and J.B. Clark, The Mg-Sn (Magnesium-Tin) System, *Bull. Alloy Phase Diagr.*, 1984, **5**, p 466–476.
6. C.L. Mendis, C.J. Bettles, M.A. Gibson, S. Gorsse, and C.R. Hutchinson, Refinement of Precipitate Distributions in an Age-Hardenable Mg–Sn Alloy Through Microalloying, *Philos. Mag. Lett.*, 2006, **86**, p 443–456.
7. J. Zhang, S. Liu, R. Wu, L. Hou, and M. Zhang, Recent Developments in High-Strength Mg-RE-Based Alloys: Focusing on Mg-Gd and Mg-Y Systems, *J. Magnes. Alloys*, 2018, **6**, p 277–291.
8. M. Zhang, H. Zhang, A. Ma, and J. Llorca, Experimental and Numerical Analysis of Cyclic Deformation and Fatigue Behavior of a Mg-RE Alloy, *Int. J. Plast*, 2021, **139**, p 102885.
9. Y. Wu, W. Hu, and L. Sun, Elastic Constants and Thermodynamic Properties of Mg–Pr, Mg–Dy, Mg–Y Intermetallics with Atomistic Simulations, *J. Phys. D Appl. Phys.*, 2007, **40**, p 7584–7592.
10. H.K. Lim, S.W. Sohn, D.H. Kim, J.Y. Lee, W.T. Kim, and D.H. Kim, Effect of Addition of Sn on the Microstructure and Mechanical Properties of Mg–MM (Misch-Metal) Alloys, *J. Alloy. Compd.*, 2008, **454**, p 515–522.
11. T. B. Massalski, in Binary Alloy Phase Diagrams, T. B. Massalski, Ed., Second Ed. Ohio, USA: ASM International, Materials Park, 1990.
12. A. A. Nayeb-Hashemi and J. B. Clark, "Mg-Pr (Magnesium-Praseodymium)," in Phase Diagrams of Binary Magnesium Alloys, Ohio: ASM International, (1988), 252–256.
13. V.N. Eremenko, M.V. Bulanova, V.E. Listovnichii, and V.M. Petyukh, Pr-Sn, *Ukr. Khim. Zh.*, 1988, **54**, p 787–795.
14. L.P. Komarovskaya, S.A. Mykhailiv, and R.V. Skolozdra, Isothermal Section of the Pr-Cu-Sn System at 400 °C, *Russ. Metall*, 1989, **4**, p 204–288.
15. F. Weitzer, K. Hiebl, and P. Rogl, Isothermal Section of the Pr-Ag-Sn System at 400 °C, *J. Solid State Chem.*, 1992, **98**, p 291–300.
16. D. Mazzone, P. Riani, G. Zanicchi, R. Marazza, and R. Ferro, The Isothermal Section at 400 °C of the Pr-Ag-Sn Ternary System, *Intermetallics*, 2002, **10**, p 801–809.
17. J. Kim, E. Thibodeau, K. Tetley-Gerard, and I.-H. Jung, Critical Evaluation and Thermodynamic Optimization of the Sn–RE Systems: Part I. Sn–RE System (RE=La, Ce, Pr, Nd and Sm), *Calphad*, 2016, **55**, p 113–133.
18. C. Ritter, A. Provino, P. Manfrinetti, and K.A. Gschneidner, The Magnetic Structures of RMgSn Compounds (R=Ce, Pr, Nd, Tb), *J. Alloy. Compd.*, 2011, **509**, p 9724–9732.
19. P. Solokha, R. Minetti, S. De Negri, L.C.J. Pereira, A.P. Gonçalves, and A. Saccone, The RMgSn2 Series of Compounds (R = Rare Earth Metal): Synthesis, Crystal Structure, and Magnetic Measurements, *Eur. J. Inorganic Chem.*, 2017, **17**, p 3040–3047.
20. S. De Negri, P. Solokha, R. Minetti, M. Skrobańska, and A. Saccone, Isothermal Section of the La-Mg-Sn System at 500 °C and Crystal Structure of the New Ternary Stannide LaMgSn2, *J. Solid State Chem.*, 2017, **248**, p 32–39.